Soliton trains after interaction quenches in Bose mixtures

New Journal of Physics
The open access journal at the forefront of physics

Deutsche Physikalische Gesellschaft DPG
IOP Institute of Physics

Published in partnership with: Deutsche Physikalische Gesellschaft and the Institute of Physics

OPEN ACCESS

RECEIVED
5 November 2020

REVISED
12 January 2021

ACCEPTED FOR PUBLICATION
14 January 2021

PUBLISHED
16 February 2021

PAPER

Soliton trains after interaction quenches in Bose mixtures

André Cidrim[1], Luca Salasnich[2,3,4,5] and Tommaso Macrì[6,*]

[1] Departamento de Física, Universidade Federal de São Carlos, 13565-905 São Carlos, Brazil
[2] Dipartimento di Fisica e Astronomia 'Galileo Galilei', Università di Padova, via Marzolo 8, 35131 Padova, Italy
[3] INFN, Sezione di Padova, via Marzolo 8, 35131 Padova, Italy
[4] CNR-INO, via Nello Carrara, 1 - 50019 Sesto Fiorentino, Italy
[5] Padua Quantum Technologies Research Center, University of Padova, Via Gradenigo 6/b, 35131 Padova, Italy
[6] Departamento de Física Teórica e Experimental, Universidade Federal do Rio Grande do Norte, and International Institute of Physics, Natal-RN, Brazil
[*] Author to whom any correspondence should be addressed.

E-mail: macri@fisica.ufrn.br

Keywords: solitons, modulational instability, quench dynamics, multi-component BECs

Supplementary material for this article is available online

Abstract

We investigate the quench dynamics of a two-component Bose mixture and study the onset of modulational instability, which leads the system far from equilibrium. Analogous to the single-component counterpart, this phenomenon results in the creation of trains of bright solitons. We provide an analytical estimate of the number of solitons at long times after the quench for each of the two components based on the most unstable mode of the Bogoliubov spectrum, which agrees well with our simulations for quenches to the weak attractive regime when the two components possess equal intraspecies interactions and loss rates. We also explain the significantly different soliton dynamics in a realistic experimental homonuclear potassium mixture in terms of different intraspecies interaction and loss rates. We investigate the quench dynamics of the particle number of each component estimating the characteristic time for the appearance of modulational instability for a variety of interaction strengths and loss rates. Finally we evaluate the influence of the beyond-mean-field contribution, which is crucial for the ground-state properties of the mixture, in the quench dynamics for both the evolution of the particle number and the radial width of the mixture. In particular, even for quenches to strongly attractive effective interactions we do not observe the dynamical formation of solitonic droplets.

1. Introduction

Modulational instability (MI) is a generic phenomenon that consists of the spontaneous exponential growth of perturbations resulting from the interplay between nonlinearity and anomalous dispersion. MI occurs in several areas of physics. It has been observed in classical [1, 2] and quantum [3–7] fluids, in waveguides [8] and in lattices [9], as well as in nonlinear optics [10] and in charged plasmas [11].

In ultracold Bose–Einstein condensates several experimental [3–7] and theoretical [12–16] works examined the conditions for the appearance of MI. In such systems, the combination of dissipative nonequilibrium dynamics and the nonlinearity due the interactions results in MI that, after a variable time interval, induces the formation of a train of solitons [3–5, 17–19]. On the theoretical side, the far-from-equilibrium dynamics induced by an interaction quench from the repulsive regime to the attractive is usually well captured by mean-field approaches based on the solution of the Gross–Pitaevskii equation with the inclusion of dissipative three-body losses. When the BEC is confined in a quasi one-dimensional waveguide, a description based on the non polynomial nonlinear Schrödinger equation typically predicts accurately the number of solitons for relatively weak attractive interactions [5, 18–20]. The relevant scale that determines the insurgence of MI is the (inverse) most unstable wavenumber $q_{\rm MI}$. Then, one finds that the number of solitons increases monotonically with the final value of the final

scattering length. Interestingly, it is also possible to observe that the particle number of the BEC decreases with a universal power law of the holding time rescaled by the characteristic time for the creation of the modulational instability, independently of the strength of the quench [4]. Recently, the excitation spectrum of matter-wave solitons has also been measured in a quasi one-dimensional cesium condensate [21].

Whereas most works on MI in BECs focused on a single component BEC, the realization of multicomponent systems offers a natural playground to observe nonequilibrium effects in a more general framework. Restricting to two-component BECs, one notices already a rich variety of phases in the ground state. In purely repulsive mixtures, one observes a homogeneous superfluid or a phase separation when inter-species repulsion overcomes the intra-species interaction strength. In the attractive regime a series of recent experiments showed the formation of dilute self-bound droplet states in a two-component BEC both in a tight optical waveguide [22, 23] and in free space [24–26], closely following the theoretical predictions [27]. In the quasi one-dimensional geometry, upon varying the mean-field interaction from the weakly to the strongly attractive regime, one observes a smooth crossover between bright soliton states and self-bound droplets. Notably, solitons are excitations appearing genuinely in low-dimensional systems. If the one-dimensional interaction strength is attractive (focusing nonlinearity) one retrieves bright solitons, while for repulsive condensates (self-defocusing nonlinearity) one finds dark solitons. Droplets instead result from the competition between mean-field and quantum fluctuation energies with opposite sign.

Although the ground-state properties of binary BEC mixtures have been extensively investigated, the study of the conditions leading to MI in these setups has only recently received attention, both theoretically [28] and experimentally [23]. MI has been observed in the counterflow dynamics of two-component BECs in the miscible (purely repulsive) phase [25]. Also, a recent experiment with coherently coupled BECs rapidly quenched into the attractive regime reported the creation of bright soliton trains formed by dressed-state atoms [29].

In this work we thoroughly investigate the quench dynamics in a binary mixture of Bose–Einstein condensates from the repulsive to the attractive regime in an elongated quasi one-dimensional waveguide. We provide results for quenches from the repulsive to the weakly and strongly attractive regime, where solitonic states and quantum droplets respectively are expected in the ground state. We quantitatively characterize the resulting nonequilibrium dynamics by computing the number of particles and solitons as a function of the holding time after the quench. In section 2 we present a theoretical model for a two-component mixture which allows us to provide a quantitative estimate of the number of solitons following a quench dynamics based on the most unstable mode. In section 3 we discuss our numerical results. We perform simulations for the quench dynamics in three different regimes: repulsive to soliton, repulsive to droplet and soliton to droplet. Finally in section 4 we present our conclusions. In the appendix we provide some details about the ground-state phase diagram, the dynamics of the radial width of the two-component mixture, the effect of beyond-mean-field corrections on the nonequilibrium dynamics and the algorithm used to monitor the number of solitons in our simulations.

2. Model and simulations

We describe the nonequilibrium dissipative dynamics of a binary homonuclear mixture in a quasi one-dimensional waveguide with radial trapping frequency ω_r and components $i, j = 1, 2$ (with $i \neq j$) by the generalized coupled Gross–Pitaevskii equations (GPEs), which, in rescaled units, read

$$i\frac{\partial\psi_i}{\partial t} = \left(-\frac{1}{2}\nabla^2 + V(\mathbf{r}) + 4\pi\frac{a_i}{a_r}|\psi_i|^2 + 4\pi\frac{a_{ij}}{a_r}|\psi_j|^2 + \frac{128\sqrt{\pi}}{3}\frac{a_i}{a_r}\left(\frac{a_i}{a_r}|\psi_i|^2 + \frac{a_j}{a_r}|\psi_j|^2\right)^{\frac{3}{2}} - i\Gamma_i|\psi_i|^4\right)\psi_i. \tag{1}$$

Here time, energy and space are scaled in units of the inverse radial trapping frequency ω_r^{-1}, the radial trapping energy $\hbar\omega_r$ and the associated harmonic oscillator length $a_r = \sqrt{\hbar/m\omega_r}$, respectively and sum over the indices in the interaction term is assumed. The coefficients a_i and a_{ij} furnish the intra- and inter-species corresponding scattering lengths. The effective mean-field scattering length is thus given by the parameter $\delta a = a_{12} + \sqrt{a_1 a_2}$. The number of particles in each component equals $N_{1,2}$. We consider a cigar-shaped trapping harmonic potential $V(\mathbf{r}) = m\left[\omega_r^2(x^2 + y^2) + \omega_z^2 z^2\right]/2$ with frequencies $\omega_r/2\pi = 346$ Hz and $\omega_z/2\pi = 7.6$ Hz, similarly to [4], thus having a radial harmonic oscillator length of $a_r = 0.87$ μm. The generalization comes first phenomenologically including a three-body loss term $\Gamma_i = L_3^{(i)} N_i^2/(2\omega_r a_r^6)$. Following [24] we do not include mixed two-body or three-body inelastic loss rates. Secondly, in order to take into account corrections due to quantum fluctuations, we introduce the

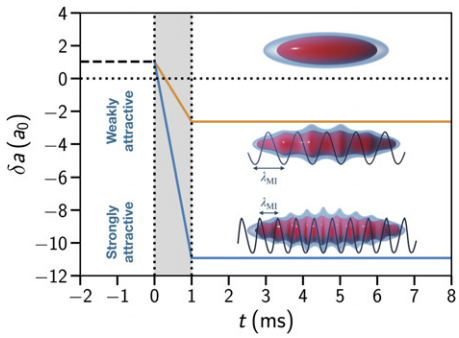

Figure 1. Quench protocol for a two-component BEC mixture from the repulsive to the attractive regime. At time $t = 0$ the effective scattering length δa is quenched using a linear ramp of the duration of $\delta t = 1$ ms from $\delta a = \delta a_{12} + \sqrt{a_{11}a_{22}} > 0$ to the attractive regime with $\delta a < 0$ either in the soliton phase or to the strongly attractive in the droplet phase. Within the same time interval we switch off the longitudinal confinement. This allows the system to expand freely and to monitor the creation of bright soliton trains propagating along the z-direction. We also consider the quench from the solitonic state to the self-bound droplet which is discussed in the text.

Lee–Huang–Yang (LHY) terms in the GPEs, with component-dependent strength. The ratio between the mean-field chemical potential and the transverse harmonic oscillator energy $(g_1 n_1 + g_2 n_2)/\hbar\omega_r \sim 1$ for typical parameters used in this work, which allows us to use consistently the three-dimensional LHY expression [30]. Note that for purely one-dimensional dynamics an attractive quantum fluctuation term would appear [28].

We perform simulations in two different regimes: (i) symmetric and (ii) realistic. In (i) we set equal initial intraspecies scattering lengths $a_{1i} = a_{2i} = 53.0a_0$ and variable final interactions with the constraint $a_{1f} = a_{2f}$, where subscripts i and f indicate values before and after quench. We also set $a_{12} = a_{12i} = a_{12f} = -52.0a_0$ and fix the three-body losses and particle numbers to the same value for each component to $L_3 = 3.6 \times 10^{-27}$ cm^6 s^{-1}. As a consequence, in this symmetric regime both components display the same density distribution at all times, i.e. $n_1 = n_1 = n$. Case (ii) is motivated by current experiments on dilute quantum droplets, with homonuclear mixtures made of two hyperfine states of ^{39}K, $|F = 1,\ m_f = 0\rangle$ and $|F = 1,\ m_f = -1\rangle$ [23, 24]. We consider the interval of magnetic fields 56 G $< B <$ 57 G, where for the two hyperfine states the intraspecies scattering lengths a_1 and a_2 are both positive (repulsive). The interspecies scattering length a_{12}, instead, is negative. In the setup we are studying the initial intra-component scattering lengths are chosen to be $a_{1i} = 75.0a_0$ and $a_2 = a_{2i} = a_{2f} = 37.5a_0$. Component 1 presents a largely varying scattering length a_1 for a particular experimentally tunable range (via Feshbach resonances), while a_2 and the inter-species scattering length $a_{12} = a_{12i} = a_{12f} = -52.0a_0$ remain practically constant for the same range [22–24]. The three-body loss rates $L_3^{(1)} = 3.6 \times 10^{-27}$ cm^6 s^{-1} and $L_3^{(2)} = 6.0 \times 10^{-29}$ cm^6 s^{-1} [24].

In the absence of a harmonic confining potential and neglecting beyond-mean-field effects one would obtain a dilute gas phase for $\delta a > 0$ and a collapsing BEC for $\delta a < 0$. The addition of the beyond-mean-field contribution to the equation of state of the two-component system leads to the stabilization of self-bound quantum droplets due to the competition of attractive mean-field terms proportional to n^2 and the repulsion due to LHY-type terms proportional to $n^{5/2}$ in the corresponding equation of state [31]. The introduction of the harmonic trap leads to a rich new physical phenomenology. The detailed ground-state phase diagram for the parameters studied in this work is described in appendix A together with the details of the numerical algorithm to obtain the ground states. The algorithm to investigate the soliton dynamics is presented in appendix D.

In most cases, when choosing initial states for our simulations, we start from repulsive inter-species interactions (i.e. $\delta a > 0$) before quenching to attractive values. The quench is performed by a rapid variation of the scattering length with a linear ramp of 1 ms. Concurrently, we switch off the longitudinal trapping potential and observe the system expanding in a time-of-flight fashion. See figure 1 for a schematic representation of the quench protocol. We also notice that the small aspect ratio of our trapping potential (i.e. $\omega_z/\omega_r \ll 1$) implies that the most relevant dynamics will happen along the axial direction. In our simulations of the GPE in equation (1) we assume cylindrical symmetry. This choice reduces the computation to an effective two-dimensional calculation of $\psi(r, z)$, over a grid size of 16×8192 points and a domain of $5a_r \times 1290a_r$ allowing to resolve in detail the dynamics along the axial direction. In order to evaluate the derivatives involved in the kinetic term, we employ a discrete (zero-order) Hankel transform in the radial direction and the usual fast Fourier transform in the longitudinal direction [32].

3. Results

3.1. Modulational instability in a binary Bose mixture

In this section we present a theoretical model to describe the MI in a binary BEC after a quench to the attractive regime $\delta a_f < 0$. To characterize quantitatively the MI we introduce the Bogoliubov spectrum for a two-component BEC, which reads [33]

$$E_{\pm}(q) = \sqrt{\frac{\varepsilon_1^2 + \varepsilon_2^2}{2} \pm \sqrt{\frac{(\varepsilon_1^2 - \varepsilon_2^2)^2}{4} + \frac{g_{12}^2 n_1 n_2 q^4}{m_1 m_2}}}, \tag{2}$$

where we defined the Bogoliubov energies of each component

$$\varepsilon_i(q) = \sqrt{\frac{q^2}{2m_i}\left(\frac{q^2}{2m_i} + g_{ii} n_i\right)}. \tag{3}$$

In this work we focus on the equal mass case $m_1 = m_2$. We define the total density of the system as $n = n_1 + n_2$. In our simulations we fix the ratio of the densities (and particle numbers) at the initial time to $\frac{n_1}{n_2} = \sqrt{\frac{a_2}{a_1}}$, i.e. the equilibrium configuration that minimizes the energy functional in the attractive regime [34]. Under the condition $\delta a = a_{12} + \sqrt{a_1 a_2} < 0$ the lower branch $E_-(q)$ becomes unstable. The most unstable mode corresponds to the wavenumber $q_{\min}$ that minimizes the argument of $E_-(q)$.

Upon solving $\mathrm{d}E_-(q)/\mathrm{d}q = 0$ we obtain

$$q_{\min}^2 = 2n\sqrt{a_1 a_2}\left(\sqrt{1 - \frac{8\,\delta a}{(\sqrt{a_1} + \sqrt{a_2})^2} + \frac{4\,\delta a^2}{\sqrt{a_1 a_2}(\sqrt{a_1} + \sqrt{a_2})^2}} - 1\right), \tag{4}$$

where we scaled the scattering lengths a_i and consequently also δa by a factor 2π to account for the effective soliton dynamics along the longitudinal direction. When $|\delta a| \ll (\sqrt{a_1} + \sqrt{a_2})^2$ then we can expand $q_{\min}$ to a reduced expression to first order in δa which reads

$$q_{\min}^2 \approx (q_{\min}^{\mathrm{red}})^2 = 8n\,|\delta a|\frac{\sqrt{a_1 a_2}}{(\sqrt{a_1} + \sqrt{a_2})^2}. \tag{5}$$

We can now define the associated wavelength $\lambda_0 = 2\pi/q_{\min}$. Starting with a quasi-1D binary Bose mixture of length L (ex. the longitudinal Thomas-Fermi radius), a sudden quench to the attractive regime induces the formation of a train of solitons. The number of solitons N_s can then be estimated as

$$N_s = \frac{L}{\lambda_0}. \tag{6}$$

3.2. Number of solitons

We now discuss the creation of soliton trains induced by the MI. In figure 2 we show snapshots of the density for the symmetric regime (i) at two different times: one right before the quench from the repulsive mean-field regime to the attractive one and another at $t = 30$ ms. Figure 2(a) corresponds to a quench to the weakly attractive regime $\delta a = -3a_0$ where the ground state of the system is an extended soliton (see appendix A for a thorough discussion of the phase diagram). Figure 2(b) corresponds to a quench to the strongly attractive regime $\delta a = -9a_0$ where the ground state is instead a self-bound droplet. For both cases the initial state is the ground state of the system for repulsive interactions. Notice that for the sake of visualization the density is normalized at its peak value, therefore the color code is the same for both components to emphasize the density modulations, even if the number of particles changes with time. We observe that, as soon as MI sets in, density peaks are formed, creating a soliton train. The number of solitons increases with the strength of the attractive interaction.

We compute the number of solitons numerically from the peaks of the density distribution for each of the two components, employing an algorithm that we describe in detail in appendix D. The results of this analysis are shown in figure 3.

In figure 3 the average number of solitons computed from the numerics (points) is compared to our prediction from equations (4) and (6) (dashed black line). We notice that the expression for $q_{\min}^{\mathrm{red}}$ in equation (5) reproduces to an excellent approximation $q_{\min}$ for the parameters used in this work. For weakly attractive interactions the agreement between the numerics and the analytical result is good for $|\delta a| \lesssim 6a_0$. For stronger attractive interactions we observe a larger deviation of the analytical prediction

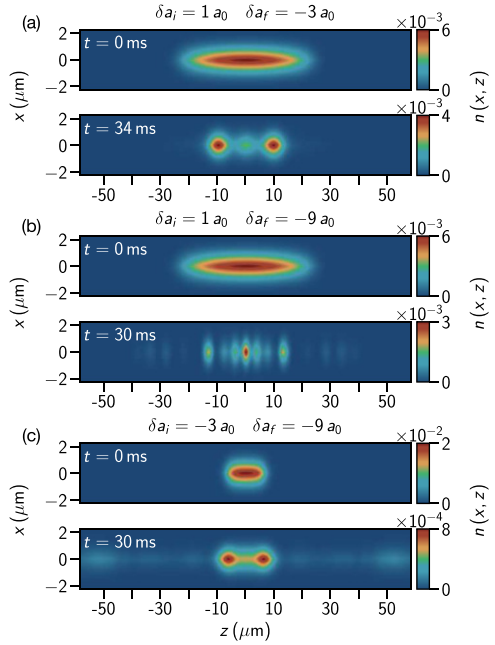

Figure 2. Snapshots of the time-evolution of the density at the initial time $t = 0$ and at $t = 30$ ms after a quench with a 1 ms-ramp for different initial and final scattering lengths. We consider the initial number of particles $N_1 = N_2 = 2.5 \times 10^4$ and symmetric intraspecies interactions $a_1 = a_2$ which are quenched simultaneously. The interspecies scattering length a_{12} is left unaltered during the quench. The system is initialized in the ground state for the corresponding value of δa_i by relaxing in imaginary time a variational gaussian wavefunction. For details of the numerical algorithm and the initial ground-state function see appendix A. The three-body loss parameters are chosen equal to $L_3^{(1)}$. After the quench the initial state develops an MI toward the soliton train visible at longer times. (a) Quench from the repulsive ground state at $\delta a_i = 1a_0$ to the soliton regime at $\delta a_f = -3a_0$. (b) Quench to the droplet phase at $\delta a_f = -9a_0$. (c) Quench from the soliton $\delta a_i = -3a_0$ to the droplet phase at $\delta a_i = -9a_0$. See supplementary material (https://stacks.iop.org/NJP/23/023022/mmedia) for videos showing the full dynamics of the three cases presented here.

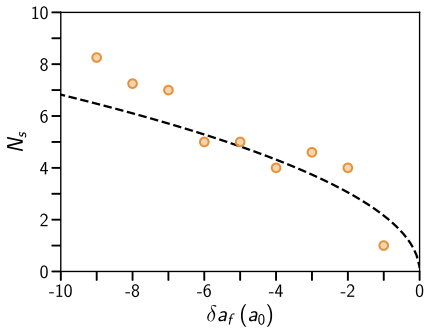

Figure 3. Number of bright solitons in quench dynamics as a function of the final value of the effective scattering length δa_f for a symmetric mixture with equal intraspecies interactions and dissipations. Solitons are identified from counting density peaks after radial integration. We compare the numerical results with the estimate of the number of solitons from equations (4) and (6) (black dashed line). We set $N_1 = N_2 = 2.5 \times 10^4$ particles with $\omega_r/2\pi = 346$ Hz and $\omega_z/2\pi = 7.6$ Hz and $L_3^{(1)} = L_3^{(2)} = 3.6 \times 10^{-27}$ cm^6 s^{-1}. Here we set $a_{12} = -52a_0$ and vary $a_1 = a_2$, computing then $\delta a = \delta a_{12} + \sqrt{a_1 a_2}$. The dynamics is initialized in the ground state with a repulsive BEC with $a_1 = a_2 = 53a_0$.

from the numerics, likely due to the far from equilibrium dynamics involved in the creation of the soliton train.

In figure 2(c) we show the snapshot of the density starting from a solitonic, weakly attractive configuration to the regime of strong attraction. We observe that the initial condensate splits into just two bright solitons. This has to be compared to figure 2(b), where, due to the larger initial longitudinal length, the quench dynamics produces a soliton train with several density peaks.

We also performed simulations in the realistic case (ii) for the experimental parameters of section 2. The dynamics is significantly more complex than in the symmetric case. First the asymmetry in the number of particles (see section 3.3 and inset of figure 4) is such that the particles in the second component is almost constant during the expansion dynamics after the quench, whereas $N_1(t)$ is greatly reduced after tens of milliseconds, similarly to the symmetric case. The effect is that the second component is only weakly

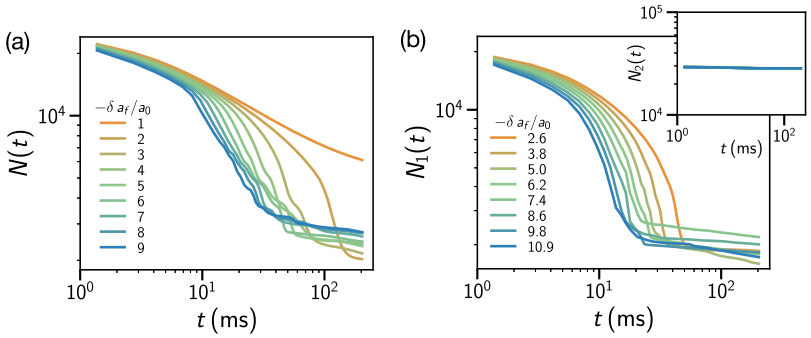

Figure 4. Time evolution for number of atoms, starting from a total $N = 5.0 \times 10^4$ particles for the case (a) of symmetric intraspecies interactions $a_1 = a_2$ and equal three-body loss coefficients $L_3^{(1)} = L_3^{(2)} = 3.6 \times 10^{-27}$ cm^6 s^{-1} and (b) realistic case of asymmetric intraspecies interactions and dissipations as described in section 2. The system is quenched from $\delta a_i = 1a_0$ to different δa_f. Notice that for realistic three-body losses coefficients $L_3^{(1)} \gg L_3^{(2)}$, therefore the second component (inset) practically maintains its particle number throughout the evolution. In (a) the dissipation acts on the two components equally, therefore $N_1(t) = N_2(t)$ for all times. Different curves in (a) and (b) correspond to different final effective interaction strength as in the color scale bar.

affected by the attractive dynamics due to the limited overlap with the first component. Therefore the soliton trains observed after the quench are poorly described by the theory presented in section 3. We provide further details in appendix D.

3.3. Number of atom loss

In this section we discuss the evolution of the number of particles as a function of time after the quench. In figure 4 we show the results for both quantities from GPE simulations of the two coupled components $N_1(t)$ and $N_2(t)$ for (a) the case of symmetric interactions and losses (b) and for the realistic experimental parameters of section 2. In the symmetric case $N_1(t) = N_2(t)$ for all times, whereas in the realistic case the number of particles in components 1 and 2 decrease with time at different rates because of the different three-body losses coefficients $L_3^{(1)}, L_3^{(2)}$. The first component has a much larger three-body decay, resulting in a more complex dynamics. We observe that for all the final attractive mean-field interactions considered in figure 4, the number of particles for short times slowly decreases before establishing the MI at $t \approx t_{\rm MI}$

$$t_{\rm MI}\,\omega_r = \frac{(\sqrt{a_1}+\sqrt{a_2})^2}{\sqrt{a_1 a_2}}\frac{1}{4n_0|\delta a|a_r^2}, \tag{7}$$

where n_0 is the peak density of the initial configuration [20]. Consistently with the prediction of equation (7), in our simulations for the symmetric (a) and the realistic case (b), quenching to the strongly attractive regime leads to faster decrease of the particle number.

4. Conclusions

In this work we studied the nonequilibrium dynamics of a two-component Bose–Einstein condensate after a quantum quench to the attractive interspecies interactions. We specialized to the experimentally relevant case of potassium binary mixture. Quenching the effective mean-field scattering length from repulsive to attractive values in a wide interval we observed an MI and the creation of soliton trains. We characterized quantitatively the number of solitons via numerical simulations of the coupled Gross–Pitaevskii equations. In the stationary, long-time limit we observed that an analytical model based on the calculation of the most unstable Bogoliubov mode is in reasonable quantitative agreement with the number of solitons for both components in the symmetric configuration. The experimentally relevant case, with asymmetric intraspecies interactions and different loss rates, leads to a more intricate dynamics which is only qualitatively captured by our model. The related time scale for the rise of the instability however does not translate into a universal scaling for the losses of both components, in contrast to what was recently observed for a single component lithium BEC with small final scattering length $|a_f|$ [4].

We emphasize that this work focuses on a far-from-equilibrium dynamical regime. For the fast magnetic field ramps considered here, even in the strongly attractive regime $|\delta a_f| \gtrsim 7a_0$, the solitonic bumps in the density are not self-bound droplets, as their width equals the transverse harmonic oscillator length and the atom number decay is different from what has been observed in the formation of self-bound droplets [34] (see also appendix B).

The MI analysis can be used to study also other Bose-condensed systems. A sudden quench of the s-wave scattering length can be applied not only to atomic gases in the same or different hyperfine states, but also to heteronuclear bosonic mixtures. Moreover, in bosonic systems with spin–orbit and Rabi couplings the MI can be induced by varying these one-body couplings. However, our work strongly suggests that generically one cannot trust only the analytical calculations based on the most unstable mode of the elementary excitations: a comparison with numerical simulation is needed to obtain reliable predictions. Extensions of this work may include a systematic study on the effects of coherently coupling a two-components mixture [29, 35, 36], the inclusion of long-range dipolar interactions [37], or the investigation of finite-temperature effects [38] across the normal-to-BEC transition in the attractive regime and its connection to the Kibble–Zurek mechanism [39, 40].

Acknowledgments

We thank D Luo, R Hulet, and S Wüster for useful discussions. This research was developed with the help of XMDS2 software [41]. We thank the High Performance Computing Center (NPAD) at UFRN for providing computational resources. TM acknowledges CNPq for support through Bolsa de produtividade em Pesquisa n.311079/2015-6. This work was supported by the Serrapilheira Institute (Grant No. Serra-1812-27802), CAPES-NUFFIC Project No. 88887.156521/2017-00. TM thanks the Physics Department of the University of L'Aquila for the hospitality where part of the work was done. AC is supported by FAPESP through Grant No. 2017/09390-7. LS acknowledges the BIRD project 'Superfluid properties of Fermi gases in optical potentials' of the University of Padova for financial support.

Data availability statement

The data that support the findings of this study are available upon reasonable request from the authors.

Appendix A. Ground-state phase diagram

In this appendix we discuss the ground-state properties of a two-component mixture in the attractive regime in a cigar-shaped harmonic potential. In figure A1 we show the numerical and the variational phase diagram obtained by imaginary-time evolution of the generalized GPE of equation (1) (numerical) and by minimizing the corresponding energy functional (variational). For the variational approach we employ a Gaussian wavefunction

$$\psi(\mathbf{r}) = \sqrt{\frac{N}{\pi^{\frac{3}{2}}\sigma_r^2\sigma_z}}\,\exp\left(-\sum_{r_i=x,y,z}\frac{r_i^2}{2\sigma_{r_i}^2}\right), \tag{A.1}$$

with variational parameters σ_r and σ_z. The wavefunction is normalized to the total number of particles $\|\psi\|^2 = N$ [31].

We observe a smooth crossover from the droplet to the soliton phase. First, for low particle number or, equivalently, small values of $|\delta a|$, the ground state of the system corresponds to a soliton, whose shape depends on the external trapping, for which $\sigma_r \sim a_r$, while $\sigma_z \gg a_r$. Specifically, beyond-mean-field corrections are not necessary for the stability of this state [20]. Reducing δa the ground state is (almost) isotropic $\sigma_r \sim \sigma_z < a_r$, independent of the confinement aspect ratios. The existence of this self-bound state is enabled by taking into account the contribution of Gaussian quantum fluctuations in the variational energy equation (1).

We compare the ground states obtained from the variational analysis with the numerical simulation of the GP equation. After relaxation in imaginary time, we find that the ground state of the system for the strongly attractive inter-species scenario is a self-trapped, spherical droplet state.

Appendix B. Evolution of the radial width

The results of the dynamics of the radial widths of each of the two components of the mixture after the quench are shown in figure B1. The radii of both components fluctuate closely to the initial radial harmonic oscillator length a_r for both quenches to the weakly attractive and strongly attractive regimes. In particular, for the cases where $\delta a_f = -9.0a_0$ (symmetric) $\delta a_f = -10.92a_0$ (realistic) and which have a self-bound droplet phase as a ground state (see figure A1) we observe no signature of such a state throughout the dynamics.

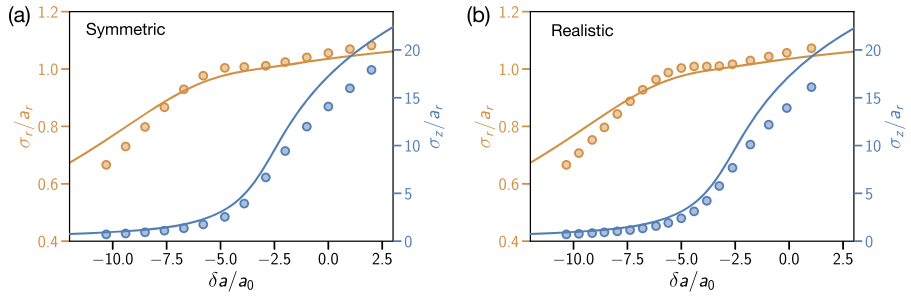

Figure A1. Crossover soliton-droplet as a function of the effective scattering length for a two-component mixture with $N = 5.0 \times 10^4$ particles with $\omega_r/2\pi = 346$ Hz and $\omega_z/2\pi = 7.6$ Hz. Orange line: σ_r, blue line: σ_z in units of a_r. (a) Symmetric case. We set $a_{12} = -52a_0$ and vary $a_1 = a_2$, so as to effectively vary $\delta a = \delta a_{12} + \sqrt{a_1 a_2}$. (b) Realistic experimental case. We fix $a_1 = 37.5a_0$ and $a_{12} = -52.0a_0$ and vary a_2. For large negative δa the system is in the droplet phase $\sigma_r \sim \sigma_z \ll a_r$. For small negative δa the system is in the soliton phase $\sigma_r \sim a_r < \sigma_z$. Numerical simulation of the ground state wavefunction obtained by imaginary-time evolution of the generalized GPE of equation (1) in the absence of dissipation are shown with orange (σ_r) and blue (σ_z) points.

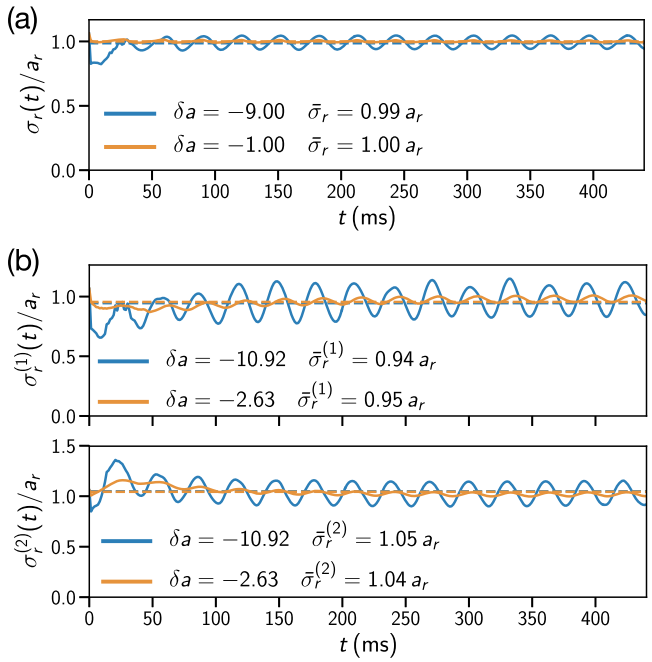

Figure B1. Time evolution of the radial widths after integrating along the longitudinal direction for the (a) symmetric and (b) realistic experimental case. In the realistic experimental case (b) we plot the time evolution for component 1 (upper panel) and component 2 (lower panel). We consider a two-component mixture with $N = 5.0 \times 10^4$ particles with $\omega_r/2\pi = 346$ Hz. We notice that, independently of the quench parameters, the radial widths oscillate around the harmonic potential length (a_r).

Appendix C. Effect of quantum fluctuations

The effect of the quantum fluctuations for two-component Bose gas is described by the term $g_i^{\mathrm{LHY}} = \frac{128\sqrt{\pi}}{3}\frac{a_i}{a_r}\left(\frac{a_i}{a_r}|\psi_i|^2 + \frac{a_j}{a_r}|\psi_j|^2\right)^{\frac{3}{2}}$ in the extended GPE equation (1). We tested the effect of removing this term in our simulations for quenches into the weak and strong attractive regime. The results are shown in figure C1 for symmetric interactions and loss terms and for the realistic experimental configuration. Whereas the results for the second component in the realistic case are almost identical, the first component displays a much faster particle number decay in the absence of beyond-mean-field terms. This can be explained by the attractive nature of the mean-field interaction which is not balanced by the additional repulsive LHY correction leading to higher densities and therefore to higher losses. At the same time, MI takes place on a shorter time scale, leading to a faster stabilization of the particle number. Therefore, at longer times, in the absence of beyond-mean-field effects we observe a larger particle number.

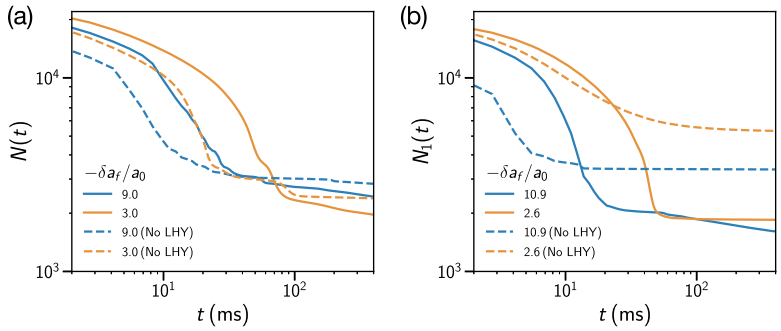

Figure C1. Effect of beyond-mean-field corrections on the dynamics of the particle number decay after the quench for (a) the symmetric case, with equal interactions $a_1 = a_2$ and loss rates $L_3^{(1)} = L_3^{(1)}$, and (b) the realistic experimental case, with the parameters of section 2. Full lines: simulation with LHY correction. Dashed lines: simulations without LHY correction. In (b) we only show $N_1(t)$ as N_2 remains constant for the whole time interval.

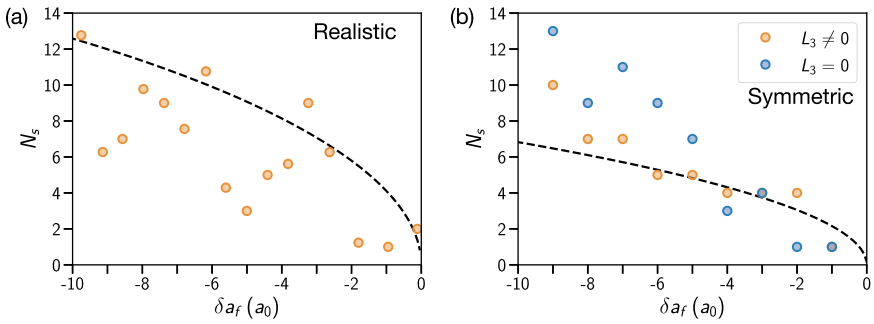

Figure D1. Number of solitons for $N = 5 \times 10^4$ in the (a) realistic and (b) symmetric cases. The latter compares the effect of disregarding the three-body losses.

Appendix D. Details on the soliton number algorithm and comparison with theory

We briefly describe the algorithm to compute the number of solitons from the dynamics of the density $n(z, t)$ integrated along the transverse directions as a function of time. Our method identifies local maxima in $n(z, t)$ as bright solitons. We start by disregarding, at each instant, peaks in low-density regions (with amplitudes $\lesssim 10\%$ of the mean initial density). A weak Gaussian filter is applied to smooth out most numerical effects at distances much smaller than the typical healing length ξ of the system. Finally, we avoid overcounting solitons which are undergoing a probable splitting process by treating as one visible peaks that are apart by distances smaller than ξ at a particular instant.

In figure D1 we provide further numerical results about the comparison between the realistic and the symmetric case with our theoretical model. In the realistic case, as discussed in the main text, we only plot the number of solitons in the first component N_s^1. The dynamics in the realistic case is significantly more complex than in the symmetric one. Therefore the soliton trains observed after the quench are inadequately described by the theory in this context. Due to this poor agreement between the numerics and the estimate from equation (6), we only show the effect of three-body losses on the solitons number in the more controllable symmetric case. We observe that in the absence of losses equation (6) is still able to provide a reasonable estimate of the number of solitons for quenches to intermediate values of $|\delta a_f|$. However, for larger $|\delta a_f|$ the deviation can be as much as 100%. In the realistic case it can be argued that a similar increase in the number of solitons might be observed in the absence of dissipation, therefore partially compensating for the mismatch of the theoretical (dashed line) and the numerics. However a more refined theory is needed to explain the behavior of both components.

ORCID iDs

André Cidrim https://orcid.org/0000-0003-0007-2330
Luca Salasnich https://orcid.org/0000-0003-0817-4753
Tommaso Macrì https://orcid.org/0000-0002-7778-8014

References

[1] Benjamin T B and Feir J E 1967 The disintegration of wave trains on deep water part 1. Theory *J. Fluid Mech.* **27** 417–30
[2] Yuen H C and Lake B M M 1980 Instabilities of waves on deep water *Annu. Rev. Fluid Mech.* **12** 303–34
[3] Strecker K E, Partridge G B, Truscott A G and Hulet R G 2002 Formation and propagation of matter-wave soliton trains *Nature* **417** 150–3
[4] Nguyen J H V, Luo D and Hulet R G 2017 Formation of matter-wave soliton trains by modulational instability *Science* **356** 422–6
[5] Everitt P J *et al* 2017 Observation of a modulational instability in bose-einstein condensates *Phys. Rev.* A **96** 041601
[6] Mežnaršič T, Arh T, Brence J, Pišljar J, Gosar K, Gosar Ž, Žitko R, Zupanič E and Jeglič P 2019 Cesium bright matter-wave solitons and soliton trains *Phys. Rev.* A **99** 033625
[7] Carr L D and Castin Y 2002 Dynamics of a matter-wave bright soliton in an expulsive potential *Phys. Rev.* A **66** 063602
[8] Tai K, Hasegawa A and Tomita A 1986 Observation of modulational instability in optical fibers *Phys. Rev. Lett.* **56** 135–8
[9] Fort C, Cataliotti F S, Fallani L, Ferlaino F, Maddaloni P and Inguscio M 2003 Collective excitations of a trapped bose-einstein condensate in the presence of a 1d optical lattice *Phys. Rev. Lett.* **90** 140405
[10] Agrawal G 2019 *Nonlinear Fiber Optics* (New York: Academic)
[11] Thornhill S G and ter Haar D 1978 Langmuir turbulence and modulational instability *Phys. Rep.* **43** 43–99
[12] Salasnich L, Parola A and Reatto L 2003 Modulational instability and complex dynamics of confined matter-wave solitons *Phys. Rev. Lett.* **91** 080405
[13] Smerzi A, Trombettoni A, Kevrekidis P G and Bishop A R 2002 Dynamical superfluid-insulator transition in a chain of weakly coupled bose-einstein condensates *Phys. Rev. Lett.* **89** 170402
[14] Carr L D and Brand J 2004 Pulsed atomic soliton laser *Phys. Rev.* A **70** 033607
[15] Karpiuk T, Brewczyk M, Ospelkaus-Schwarzer S, Bongs K, Gajda M and Rzażewski K 2004 Soliton trains in bose-fermi mixtures *Phys. Rev. Lett.* **93** 100401
[16] Gori G, Macrì T and Trombettoni A 2013 Modulational instabilities in lattices with power-law hoppings and interactions *Phys. Rev.* E **87** 032905
[17] Al Khawaja U, Stoof H T C, Hulet R G, Strecker K E and Partridge G B 2002 Bright soliton trains of trapped bose-einstein condensates *Phys. Rev. Lett.* **89** 200404
[18] Mistakidis S I *et al* 2018 Correlation effects in the quench-induced phase separation dynamics of a two species ultracold quantum gas *New J. Phys.* **20** 043052
[19] Kiehn H, Mistakidis S I, Katsimiga G C and Schmelcher P 2019 Spontaneous generation of dark-bright and dark-antidark solitons upon quenching a particle-imbalanced bosonic mixture. *Phy. Rev.* A **100** 023613
[20] Salasnich L, Parola A and Reatto L 2002 Condensate bright solitons under transverse confinement *Phys. Rev.* A **66** 043603
[21] Di Carli A, Colquhoun C D, Henderson G, Flannigan S, Oppo G-L, Daley A J, Kuhr S and Haller E 2019 Excitation modes of bright matter-wave solitons *Phys. Rev. Lett.* **123** 123602
[22] Cabrera C R, Tanzi L, Sanz J, Naylor B, Thomas P, Cheiney P and Tarruell L 2018 Quantum liquid droplets in a mixture of bose-einstein condensates *Science* **359** 301–4
[23] Cheiney P, Cabrera C R, Sanz J, Naylor B, Tanzi L and Tarruell L 2018 Bright soliton to quantum droplet transition in a mixture of bose-einstein condensates *Phys. Rev. Lett.* **120** 135301
[24] Semeghini G *et al* 2018 Self-bound quantum droplets of atomic mixtures in free space *Phys. Rev. Lett.* **120** 235301
[25] Hamner C, Chang J J, Engels P and Hoefer M A 2011 Generation of dark-bright soliton trains in superfluid-superfluid counterflow *Phys. Rev. Lett.* **106** 065302
[26] D'Errico C, Burchianti A, Prevedelli M, Salasnich L, Ancilotto F, Modugno M, Minardi F and Fort C 2019 Observation of quantum droplets in a heteronuclear bosonic mixture *Phys. Rev. Res.* **1** 033155
[27] Petrov D S 2015 Quantum mechanical stabilization of a collapsing bose-bose mixture *Phys. Rev. Lett.* **115** 155302
[28] Mithun T, Maluckov A, Kasamatsu K, Malomed B A and Khare A 2020 Modulational instability, inter-component asymmetry, and formation of quantum droplets in one-dimensional binary bose gases *Symmetry* **12** 174
[29] Sanz J, Frölian A, Chisholm C S, Cabrera C R and Tarruell L 2019 Interaction control and bright solitons in coherently-coupled Bose–Einstein condensates (arXiv:1912.06041)
[30] Zin P Ł, Pylak M, Wasak T, Gajda M and Idziaszek Z 2018 Quantum Bose–Bose droplets at a dimensional crossover *Phys. Rev.* A **98** 051603
[31] Cappellaro A, Macrì T and Salasnich L 2018 Collective modes across the soliton-droplet crossover in binary Bose mixtures *Phys. Rev.* A **97** 053623
[32] The zero-order Hankel transform of a function $f(r, z)$ is given by $\tilde{f}(k_r, k_\phi, z) = -2i\pi \int_0^\infty f(r, z) J_0(k_r r) r dr$. The full momentum-space representation of $f(r, z)$ is then $\tilde{f}(\mathbf{k}) = F_z[\tilde{f}(k_r, k_\phi, z]$, with $F_z[\cdot]$ the usual Fourier transform along the z-direction.
[33] Larsen D M 1963 Binary mixtures of dilute bose gases with repulsive interactions at low temperature *Ann. Phys., NY* **24** 89–101
[34] Ferioli G, Semeghini G, Terradas-Briansó S, Masi L, Fattori M and Modugno M 2020 Dynamical formation of quantum droplets in a ^{39}K mixture *Phys. Rev. Res.* **2** 013269
[35] Cappellaro A, Macrì T, Bertacco G F and Salasnich L 2017 Equation of state and self-bound droplet in rabi-coupled bose mixtures *Sci. Rep.* **7** 13358
[36] Bhat I A, Mithun T, Malomed B A and Porsezian K 2015 Modulational instability in binary spin-orbit-coupled bose-einstein condensates *Phys. Rev.* A **92** 063606
[37] Ferrier-Barbut I, Wenzel M, Schmitt M, Böttcher F and Pfau T 2018 Onset of a modulational instability in trapped dipolar bose-einstein condensates *Phys. Rev.* A **97** 011604
[38] Lee K L, Jørgensen N B, Wacker L J J, Skou M G G, Skalmstang K T T, Arlt J J J and Proukakis N P P 2018 Time-of-flight expansion of binary Bose-Einstein condensates at finite temperature *New J. Phys.* **20** 053004
[39] Comaron P, Larcher F, Dalfovo F and Proukakis N P 2019 Quench dynamics of an ultracold two-dimensional Bose gas *Phys. Rev.* A **100** 033618
[40] Chen Y, Horikoshi M, Yoshioka K and Kuwata-Gonokami M 2019 Dynamical critical behavior of an attractive bose-einstein condensate phase transition *Phys. Rev. Lett.* **122** 040406
[41] Dennis G R, Hope J J and Johnsson M T 2013 XMDS2: fast, scalable simulation of coupled stochastic partial differential equations *Comput. Phys. Commun.* **184** 201–8